COMMUNICATIONS IN NUMERICAL METHODS IN ENGINEERING
Commun. Numer. Meth. Engng 2000; **16**:657–670

On the sensitivity of homogenized material responses at infinitesimal and finite strains

T. I. Zohdi* and P. Wriggers

Institut für Baumechanik und Numerische Mechanik, Appelstrasse 9A, 30167 Hannover, Germany

SUMMARY

On a practical level, when computing macroscopic or *homogenized* mechanical responses of materials possessing heterogeneous irregular microstructure, one can only test finite-sized samples. The macroscopic responses computed from various equal finite-sized samples exhibit deviations from one another. Consequently, any use of such data afterwards contains a degree of uncertainty. For example, certain classes of finite deformation response functions such as compressible Neo-Hookean functions, compressible Mooney–Rivlin functions, and others, employ predetermined linear elastic coefficients in parts of their representations. Therefore, they will contain the mentioned uncertainties. In this work we study the magnitude of deviations between computed homogenized linearly elastic responses among equal finite sized, samples possessing random microstructure. Afterwards, the sensitivity of finite deformation response functions to such deviations is addressed. The primary result is that deviations of the responses in the infinitesimal range bound the resulting perturbed response in the finite deformation range from above. Copyright © 2000 John Wiley & Sons, Ltd.

KEY WORDS: homogenized responses; perturbations; hyperelasticity; finite deformations

1. INTRODUCTION

A primary research issue in the analysis of solid microheterogeneous materials is the determination of 'effective' or 'homogenized' constitutive laws for use in macroscopic structural calculations. The usual approach is to determine a relation between averages, $\mathbb{E}^*$, defined through $\langle \boldsymbol{\sigma} \rangle_\Omega = \mathbb{E}^* : \langle \boldsymbol{\varepsilon} \rangle_\Omega$. Here, $\langle \cdot \rangle_\Omega \stackrel{\text{def}}{=} 1/|\Omega| \int_\Omega \mathrm{d}\Omega$, and $\boldsymbol{\sigma}$ and $\boldsymbol{\varepsilon}$ are the stress and strain fields within a statistically representative volume element (RVE) with volume $|\Omega|$. If $\mathbb{E}^*$ is assumed isotropic one may write

$$3\kappa^* \stackrel{\text{def}}{=} \frac{\langle \operatorname{tr} \boldsymbol{\sigma}/3 \rangle_\Omega}{\langle \operatorname{tr} \boldsymbol{\varepsilon}/3 \rangle_\Omega} \quad \text{and} \quad 2\mu^* \stackrel{\text{def}}{=} \sqrt{\frac{\langle \boldsymbol{\sigma}' \rangle_\Omega : \langle \boldsymbol{\sigma}' \rangle_\Omega}{\langle \boldsymbol{\varepsilon}' \rangle_\Omega : \langle \boldsymbol{\varepsilon}' \rangle_\Omega}} \tag{1}$$

where $\operatorname{tr} \boldsymbol{\sigma}$ and $\operatorname{tr} \boldsymbol{\varepsilon}$ are the dilatational components of the stress and strain and where $\boldsymbol{\sigma}'$ and $\boldsymbol{\varepsilon}'$ are the deviatoric stresses and strains. We note that even if the aggregate response is not purely isotropic, one can always interpret the above expressions as generalizations of isotropic

*Correspondence to: T. I. Zohdi, Institut für Baumechanik und Numerische Mechanik, Universität Hannover, Appelstrasse 9A, 30167 Hannover, Germany

Received 19 November 1999
Accepted 10 May 2000

responses. In theory, an effective response will be invariant for a sample that is infinitely large compared to the microstructure. However, from a practical point of view, whether computationally or experimentally, we can only test finite-sized samples of material. Therefore, equal-sized finite samples will produce $\mathbb{E}^*$'s that exhibit deviations from one another. Clearly, no single effective response appears. Therefore, in the case of overall isotropic responses, we have uncertainties, such as $\mu^* \pm \Delta\mu^*$ and $\kappa^* \pm \Delta\kappa^*$. The determination of the magnitude of such uncertainties is the subject of this work. In particular, because of the widespread use of lightweight polymeric materials, the determination of their accurate responses is necessary in many applications. In this work, our interest is in the response of porous polyethelenes. Polyethelenes and related polymers have the largest volume use of any plastic in the world. They are prepared by the catalytic polymerization of ethelyene. Depending on the mode of polymerization, one can obtain a high-density (HDPE) or a low-density (LDPE) polyethelene polymer. A common use of LDPEs is for lightweight packaging. Such porous polyethelenes can readily be prepared and are characterized by excellent low thermal conductivity, high strength-to-weight ratio, low water absorption, and high energy absorption. These attributes have made such porous polyethelenes of special interest as insulation boards for construction, protective packaging materials, insulated drinking cups, and floatation devices. For more details on applications see the well-known text of Gibson and Ashby [1]. In many manufacturing processes such materials are obtained by chemically treating a vulcanized polymer, which results in a fine distribution of pores or extremely soft inclusions, throughout the material. Such porous polymeric materials are expected to undergo finite deformations. Certain classes of models to describe the mechanical responses of such materials are constructed from the linearly elastic coefficients. Therefore, if one is to construct an admissible effective finite deformation response function from the linearly elastic responses an uncertainty enters. Therefore, we also study the effects of the perturbations when used in finite deformation response functions, with examples focusing on modelling compressible porous polyethelenes. A widely used class of models are the compressible Neo-Hookean and compressible Mooney–Rivlin material response functions.

The outline of the paper is as follows. In Section 2 a brief summary of the linear theory of effective properties is given, and numerical tests are performed varying the ratio of sample size to micro-particle/pore diameter. In Section 3 finite deformation responses are developed that employ material parameters obtained in Section 2 are given. In Section 4 the sensitivity of the finite deformation response to perturbations in the linearly elastic effective constants are developed. Finally, in Section 5 a summary and concluding remarks are given.

2. QUANTIFYING PERTURBATION MAGNITUDES

When determining effective responses, the basic assumptions are (1) the RVE geometry is a scale smaller than that of the macroscopic body (and the macroscopic external loading) such that it can be considered as a 'material point' that can only 'see' uniform boundary loading and (2) the length scales of the microconstituents are a scale smaller than the RVE geometry thus allowing negligibly small fluctuations of microfields in relation to the RVE length scale. A concise statement of such size requirements placed on the RVE is $\langle \boldsymbol{\sigma} : \boldsymbol{\varepsilon} \rangle_\Omega = \langle \boldsymbol{\sigma} \rangle_\Omega : \langle \boldsymbol{\varepsilon} \rangle_\Omega$, where $\boldsymbol{\sigma}$ and $\boldsymbol{\varepsilon}$ are the stress and strain tensor fields within a statistically representative volume element (RVE) with volume $|\Omega|$. This is known as Hill's condition (for example see Reference [2] or [3]). A special class of fields, referred to as 'uniform', that fall under Hill's condition are those produced in bodies

with applied boundary data of the following forms: (1) pure linear displacements in the form $\mathbf{u}|_{\partial\Omega} = \mathscr{E} \cdot \mathbf{x}$ and (2) pure tractions in the form $\mathbf{t}|_{\partial\Omega} = \mathscr{L} \cdot \mathbf{n}$; where $\mathscr{E}$ and $\mathscr{L}$ are constant strain and stress tensors, respectively. If effective response, $\mathbb{E}^*$, is assumed isotropic, then only one test loading, containing non-zero dilatational ($\operatorname{tr}\boldsymbol{\sigma}$ and $\operatorname{tr}\boldsymbol{\varepsilon}$) and deviatoric components ($\boldsymbol{\sigma}'$ and $\boldsymbol{\varepsilon}'$), is necessary to determine the effective bulk and shear moduli (κ^* and μ^*).

2.1. Some numerical experiments with the finite element method

To model random porous microstructures, we considered a matrix containing very soft spherical nonintersecting particles/pores randomly distributed throughout a cube of dimensions $L \times L \times L$. The mechanical data $\kappa = 1.5$ GPa and $\mu = 1.0$ GPa were used for the matrix material. For simplicity we scaled down elasticity tensor's eigenvalues (κ and μ) in the particles/pores to $\frac{1}{100}$ of the matrix. The dimensions of the particles/pores were controlled such that $2r/l = 0.75$ where $l = L/N^{1/3}$, and where N is the number of particles/pores, and r is the radius of the particles/pores. This was done to keep the particle/pore volume fraction constant, which, dictated by the particle/pore dimensions, was approximately 22.5 per cent. The finite element method was employed to numerically simulate the response. The meshes employed were uniform, and repeatedly refined until no significant changes in the responses occurred. Mesh densities of approximately $9 \times 9 \times 9$ trilinear finite element hexahedra *per particle* were the final ones used. During the computations, to increase the resolution of the internal geometry, we applied a '$\frac{2}{5}$' Gauss rule, i.e. a $2 \times 2 \times 2$ Gauss rule if there was no material discontinuity in the element, and a $5 \times 5 \times 5$ rule if there is a discontinuity (Figure 2). This process, which was not the subject of this work, has been studied more in detail in Reference [4]. In these tests, the following sequence of particles/pores per sample was used: 2 (5184 DOF), 4 (10125 DOF), 8 (20577 DOF), 16 (41720 DOF), 32 (81000 DOF) and 64 (151959 DOF) particles/pores (Figures 1 and 2). In order to get more reliable response data for each sample size, the tests were performed five times and the responses averaged. Since the microstructures were random, we tracked the isotropic quantities κ^* and μ^*, as defined in Equation (1). We considered the following test loading in the infinitesimal deformation linearly elastic range:

$$\begin{bmatrix} u_1|_{\partial\Omega} \\ u_2|_{\partial\Omega} \\ u_3|_{\partial\Omega} \end{bmatrix} = \underbrace{\begin{bmatrix} \mathscr{E}_{11} & \mathscr{E}_{12} & \mathscr{E}_{13} \\ \mathscr{E}_{12} & \mathscr{E}_{22} & \mathscr{E}_{23} \\ \mathscr{E}_{31} & \mathscr{E}_{32} & \mathscr{E}_{33} \end{bmatrix}}_{\mathscr{E}} \begin{bmatrix} x_1 \\ x_2 \\ x_3 \end{bmatrix} \tag{2}$$

where $\mathscr{E}_{ij} = 0.001$, $i, j = 1, 2, 3$, throughout the tests. For the effective bulk responses a difference of approximately 6.7 per cent occurred between samples containing two particles and 64 particles samples, while a 2.6 per cent difference occurred between the effective shear responses (Table I). The following relations are the corresponding least-squares curve-fits for samples containing 2–64 particles/pores:

$$\begin{aligned} W &= 0.0001530N^{-0.0127}, & \theta^2 &= 0.953 \\ \kappa^* &= 0.8779N^{-0.0198}, & \theta^2 &= 0.965 \\ \mu^* &= 0.7841N^{-0.00702}, & \theta^2 &= 0.912 \end{aligned} \tag{3}$$

where $\theta^2 = 1.0$ is a perfect curve fit (Figures 3–5).

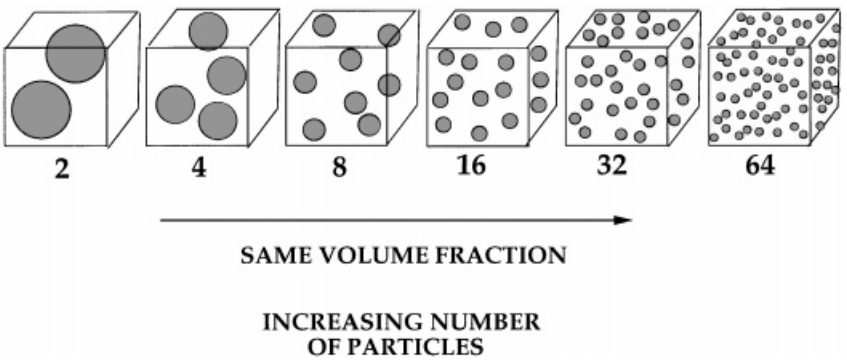

Figure 1. A series of test samples with increasingly more particles/pores, but with the volume fraction fixed.

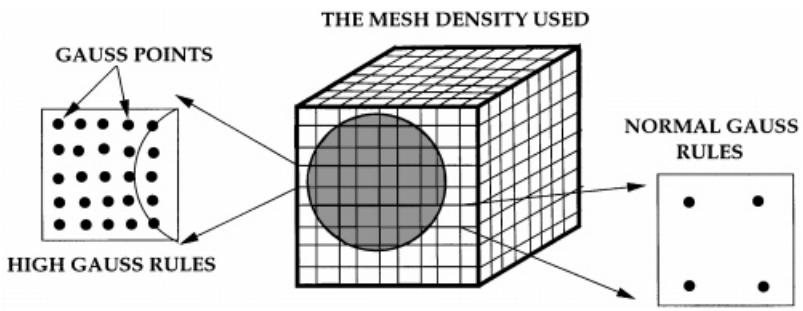

Figure 2. High mesh densities and oversampling to capture the micro-geometry.

Table I. Perturbation magnitudes for various quantities as a function of pore/particle number in the sample. Note that N is the number of pores/particles and $W_N - W_{64} \stackrel{\text{def}}{=} (\int_\Omega \nabla \mathbf{u} : \mathbb{E} : \nabla \mathbf{u} \, d\Omega)_N - (\int_\Omega \nabla \mathbf{u} : \mathbb{E} : \nabla \mathbf{u} \, d\Omega)_{64}$.

N	$W_N - W_{64}$	$\kappa_N^* - \kappa_{64}^* \stackrel{\text{def}}{=} \Delta\kappa^*$	$\frac{\kappa_N^* - \kappa_{64}^*}{\kappa_{64}^*}$	$\mu_N^* - \mu_{64}^* \stackrel{\text{def}}{=} \Delta\mu^*$	$\frac{\mu_N^* - \mu_{64}^*}{\mu_{64}^*}$
2	0.072×10^{-5}	0.055	0.067	0.020	0.026
4	0.046×10^{-5}	0.040	0.049	0.011	0.014
8	0.038×10^{-5}	0.033	0.041	0.008	0.010
16	0.015×10^{-5}	0.013	0.016	0.004	0.002
32	0.002×10^{-5}	0.002	0.002	0.001	0.001

Further tests were then carried out for a fixed sample size containing 20 randomly distributed particles/pores. This sample size selection was based upon the somewhat ad hoc fact that for three successive enlargements of samples, i.e. 16, 32 and 64 particle samples, the responses differed from one another on average by less than 1 per cent in the previous tests. We simulated 100 samples, each time with a different random distribution of 20 non-intersecting softer particles/pores

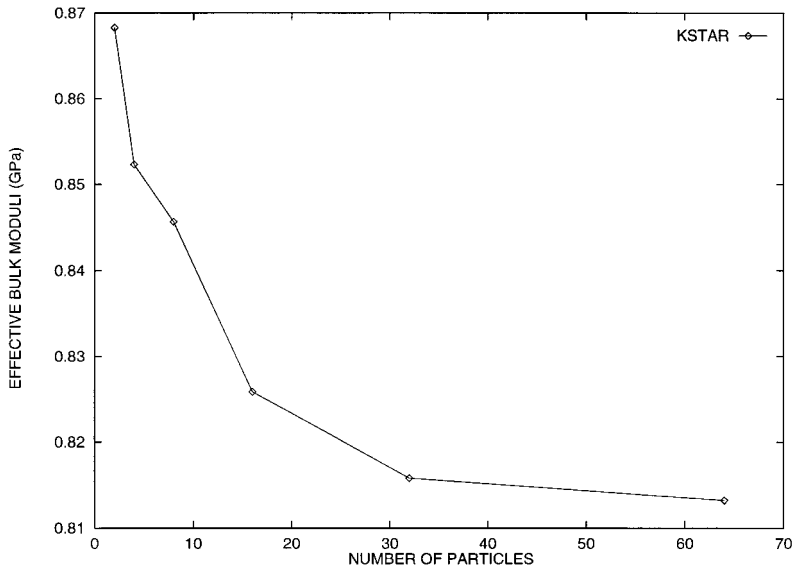

Figure 3. The values of effective bulk responses of the system for samples containing various numbers of particles/pores. Five tests were performed per sample size and averaged.

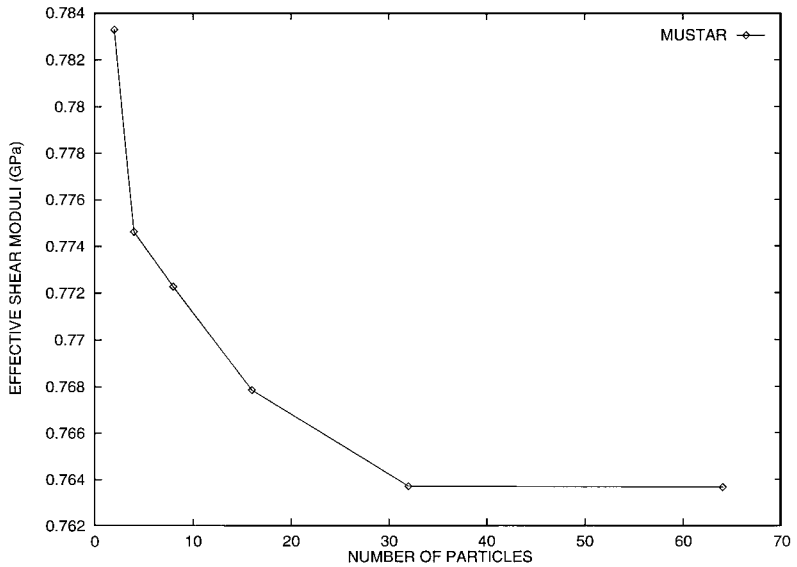

Figure 4. The values of effective shear responses of the system for samples containing various numbers of particles/pores. Five tests were performed per sample size and averaged.

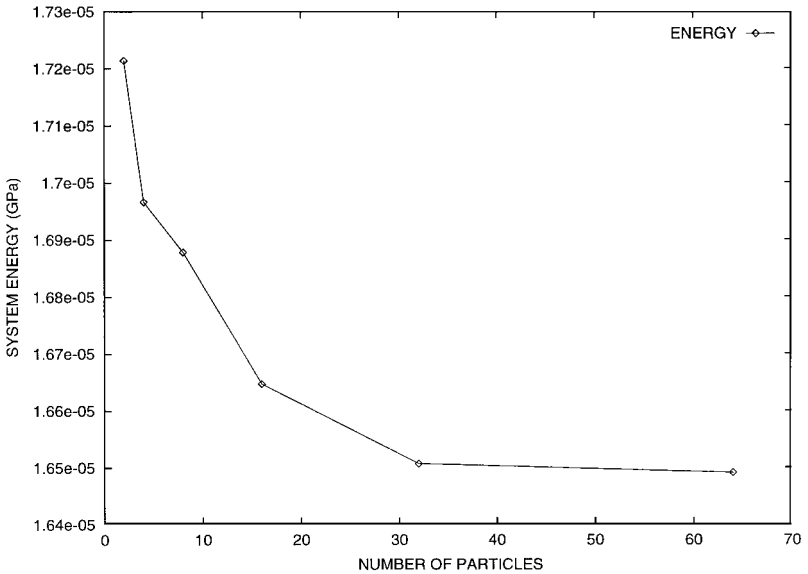

Figure 5. The values of effective energetic responses of the system for samples containing various numbers of particles/pores. Five tests were performed per sample size and averaged.

Table II. Results of 100 material tests for randomly distributed particulate microstructures.

Quantity	Average	Max–Min	Stan. dev.
$\int_\Omega \nabla \mathbf{u} : \mathbb{E} : \nabla \mathbf{u} \, d\Omega$(GPa)	0.16634×10^{-4}	0.0049×10^{-4}	0.9596×10^{-7}
κ^* (GPa)	0.8249	0.025	0.5565×10^{-2}
μ^* (GPa)	0.7674	0.023	0.4315×10^{-2}

(Table II). The loading was the same as in Equation (2) with the full matrix combined loading, $\mathscr{E}_{ij} = 0.001, \ i, j = 1, 2, 3$. Consistent with the previous tests, the mesh densities used were $9 \times 9 \times 9$ trilinear finite element hexahedra *per particle* resulting in a total $24 \times 24 \times 24$ mesh (46 875 dof per test). The results are shown in Figures 6–8. We observe that the ratio of the maximum–minimum deviations to the average for the effective bulk and shear responses, as well as the strain energy, all were approximately 3 per cent for the 20 particle samples. Each 20 particle finite element test in this paper was carried out in no more than minute on a single RISC 6000 workstation. Therefore, 100 of such tests lasted approximately two hours.

Remark. Before, continuing, we note that theoretical issues pertaining to size effects in finite-sized samples, in particular *a posteriori* bounds, have been discussed in depth in a series of papers stemming from the materials group at the Ecole Polytechnique in Lausanne: Huet [5, 6], Hazanov and Huet [7] and Hazanov and Amieur [8], as well as in a recent paper of our own, Zohdi and Wriggers [9].

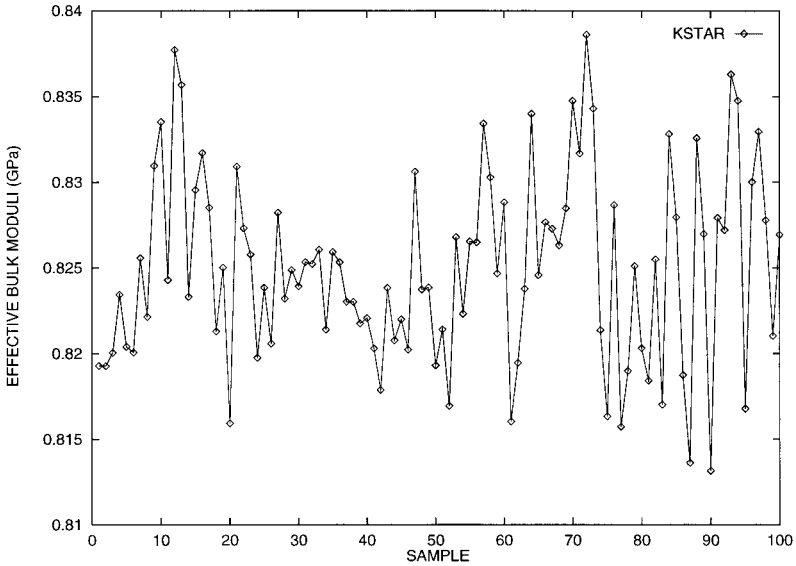

Figure 6. The values of effective bulk responses for 100 samples each containing a different distribution of random particles/pores.

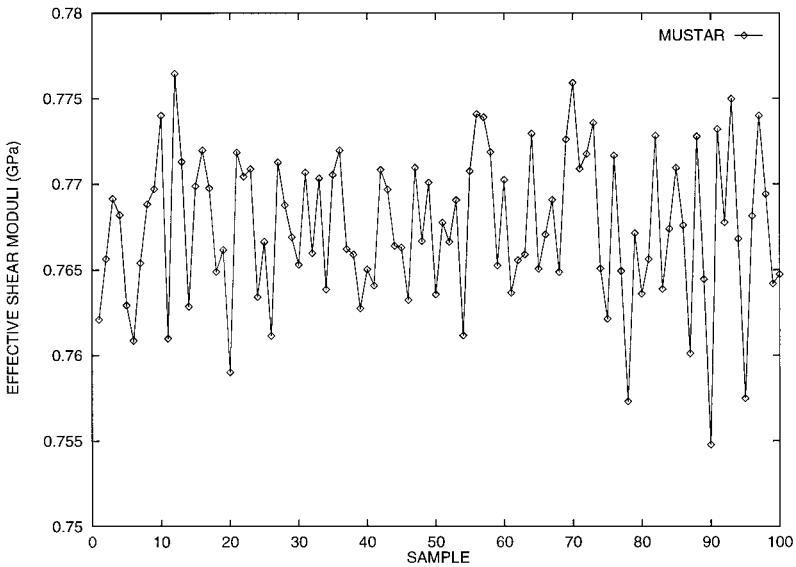

Figure 7. The values of effective shear responses for 100 samples each containing a different distribution of random particles/pores.

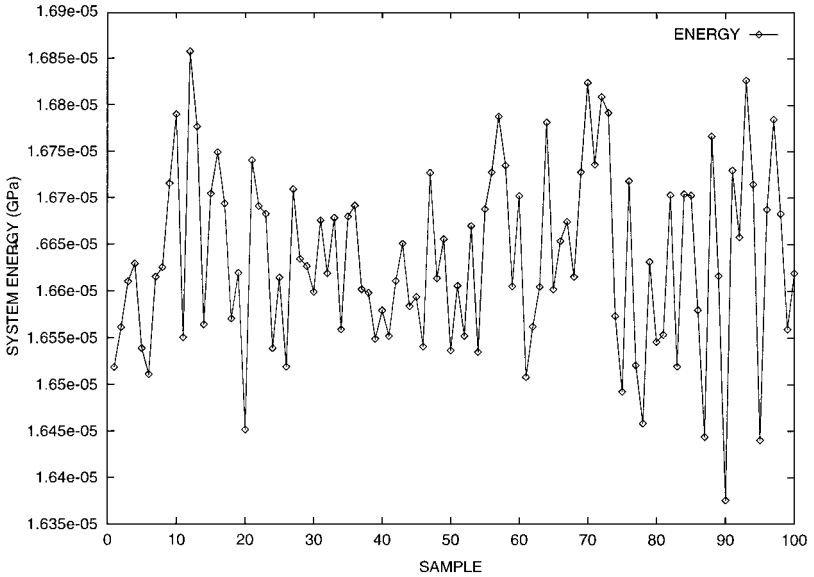

Figure 8. The values of effective energy for 100 samples each containing a different distribution of random particles/pores.

3. A PERTURBATION ANALYSIS FOR A CLASS OF FINITE DEFORMATION RESPONSE FUNCTIONS

We now address the issue of the sensitivity of finite deformation response functions to the effective property deviations observed in the previous tests. As will be seen, the primary result is that deviations of the responses in the infinitesimal range bound the resulting perturbed response in the finite deformation range from above. In the analysis to follow we choose a somewhat general standard form for a stored energy function, W

$$W = \underbrace{K_1(\overline{I}_{\mathrm{C}} - 3) + K_2(\overline{II}_{\mathrm{C}} - 3)}_{\text{incompressible part}} + \underbrace{\frac{\kappa}{2}(\sqrt{III_{\mathrm{C}}} - 1)^2}_{\text{compressible part}} \tag{4}$$

where the first and second invariants of the right Cauchy–Green tensor, $\mathbf{C} \overset{\text{def}}{=} \mathbf{F}^{\mathrm{T}} \cdot \mathbf{F}$, I_{C} and II_{C}, have been scaled by the square-root of the third invariant ($J \overset{\text{def}}{=} \det \mathbf{F} = \sqrt{III_{\mathrm{C}}}$), $\overline{I}_{\mathrm{C}} = I_{\mathrm{C}} III^{-1/3} = I_{\mathrm{C}} J^{-2/3}$, and $\overline{II}_{\mathrm{C}} = II_{\mathrm{C}} III^{-2/3} = II_{\mathrm{C}} J^{-4/3}$, to insure that they contribute nothing to the compressible part of the response. The symbol $\mathbf{F} \overset{\text{def}}{=} \partial \mathbf{x}/\partial \mathbf{X}$ is the deformation gradient, where $\mathbf{x} = \mathbf{X} + \mathbf{u}$ is the current position of a material point, $\mathbf{X}$ is the reference configuration, and $\mathbf{u}$ is the displacement of a point at $\mathbf{X}$. We recall the relation

$$\mathbf{S} = 2\frac{\partial W}{\partial \mathbf{C}} \tag{5}$$

where $\mathbf{S}=\mathbf{F}^{-1}\cdot\boldsymbol{\sigma}\cdot\mathbf{F}^{-\mathrm{T}}\mathbf{J}$ is the second Piola–Kirchoff stress, where $\boldsymbol{\sigma}$ is the Cauchy stress. Any stored energy function must obey five criteria: (**1**) $\mathbf{C}=\mathbf{I}\Leftrightarrow\mathbf{F}=\mathbf{I}\Leftrightarrow(I_{\mathrm{C}}=II_{\mathrm{C}}=3,\ III_{\mathrm{C}}=1)\Leftrightarrow W=0$, where $(I_{\mathrm{C}},II_{\mathrm{C}},III_{\mathrm{C}})$ are the principle invariants of $\mathbf{C}$, (**2**) $W\geqslant 0$, (**3**) $W\to\infty\Leftrightarrow\det\mathbf{F}\to 0$ or $\det\mathbf{F}\to\infty$, (**4**) $\mathbf{S}=\mathbf{0}$ for $\mathbf{C}=\mathbf{I}$ and (**5**) the material constants in a finite deformation material law must be adjusted so that they give hyperelastic responses with known Lame constants, $\lambda(=\kappa-2\mu/3)$ and μ, when perturbed around the undeformed configuration (see Reference [10] for more details). By satisfying conditions (1)–(5) for an admissible response function, we obtain the condition $K_1+K_2=\mu/2$. Therefore, we have in the general case

$$W=K_1(\bar{I}_{\mathrm{C}}-3)+\left(\frac{\mu}{2}-K_1\right)(\bar{II}_{\mathrm{C}}-3)+\frac{\kappa}{2}(\sqrt{III_{\mathrm{C}}}-1)^2 \tag{6}$$

In the examples to follow, we consider a convex combination decomposition

$$\frac{K_1}{2}+\frac{K_2}{2}=\phi\frac{\mu}{2}+(1-\phi)\frac{\mu}{2}=\frac{\mu}{2},\quad 0\leqslant\phi\leqslant 1 \tag{7}$$

We remark that the special case where $\phi=1$ implies that $K_1=\mu/2$ and $K_2=0$, and is denoted as a Compressible Neo-Hookean material

$$W=\frac{\mu}{2}(\bar{I}_{\mathrm{C}}-3)+\frac{\kappa}{2}(\sqrt{III_{\mathrm{C}}}-1)^2 \tag{8}$$

Now consider a finite deformation stored energy function, such as in Equation (6), that employs the effective linear elastic constants, those given in Equation (1), for its material values

$$W=K_1^*(\bar{I}_{\mathrm{C}}-3)+K_2^*(\bar{II}_{\mathrm{C}}-3)+\frac{\kappa^*}{2}(\sqrt{III_{\mathrm{C}}}-1)^2 \tag{9}$$

We refer to this expression as the effective stored energy function.

4. BOUNDS ON THE SENSITIVITY TO COEFFICIENT PERTURBATION

Our now interest is in the sensitivity of the effective response functions to perturbations in the coefficients κ^* and μ^*.

4.1. Bounds on the perturbed stored energy

In either the compressible Neo-Hookean and compressible Mooney–Rivlin case, since the stored energy function is linear in the material coefficients, we have

$$W(\kappa^*+\Delta\kappa^*)-W(\kappa^*)=\underbrace{\frac{\partial W}{\partial\kappa^*}}_{\text{bulk sensitivity}}\Delta\kappa^*\stackrel{\text{def}}{=}\xi_{\kappa^*} \tag{10}$$

and

$$W(\mu^*+\Delta\mu^*)-W(\mu^*)=\underbrace{\frac{\partial W}{\partial\mu^*}}_{\text{shear sensitivity}}\Delta\mu^*\stackrel{\text{def}}{=}\xi_{\mu^*} \tag{11}$$

In order to make meaningful comparisons of the sensitivity at various loading intensities, we normalize by the stored energy:

$$\overline{\xi_{\kappa^*}} = \frac{\xi_{\kappa^*}}{W}, \quad \overline{\xi_{\mu^*}} = \frac{\xi_{\mu^*}}{W} \tag{12}$$

We note that the normalized sensitivities, $\overline{\xi}$, are well defined at zero strain

$$\lim_{W,\xi \to 0} \frac{\xi}{W} < \infty \tag{13}$$

because the numerator and denominator tend to zero at the same rate. One can prove this using L'Hopital's rule of limits for indefinite forms such as $\lim_{x,\,y\to 0}\, x/y$.

The *sensitivities* to perturbations in the coefficients, κ^* and μ^* are

$$\frac{\partial W}{\partial \kappa^*} = \frac{1}{2}(\sqrt{III_{\mathrm{C}}} - 1)^2, \quad \frac{\partial W}{\partial \mu^*} = \frac{\phi}{2}(\overline{I}_{\mathrm{C}} - 3) + \frac{1-\phi}{2}(\overline{II}_{\mathrm{C}} - 3) \tag{14}$$

From straightforward algebraic manipulations we have

$$\boxed{\begin{gathered} |\overline{\xi_{\kappa^*}}| = \left| \frac{\Delta\kappa^*/2\mu^*(\sqrt{III_{\mathrm{C}}} - 1)^2}{\phi/2(\overline{I}_{\mathrm{C}} - 3) + (1-\phi)/2(\overline{II}_{\mathrm{C}} - 3) + \kappa^*/2\mu^*(\sqrt{III_{\mathrm{C}}} - 1)^2} \right| \leqslant \left| \frac{\Delta\kappa^*}{\kappa *} \right| \\ \operatorname*{Lim}_{III_{\mathrm{C}} \to 0} |\overline{\xi_{\kappa^*}}| = 0, \quad \operatorname*{Lim}_{III_{\mathrm{C}} \to \infty} |\overline{\xi_{\kappa^*}}| = \left| \frac{\Delta\kappa^*}{\kappa^*} \right| \end{gathered}} \tag{15}$$

and

$$\boxed{\begin{gathered} |\overline{\xi_{\mu^*}}| = \left| \frac{\Delta\mu^*/2\kappa^*(\overline{I}_{\mathrm{C}} - 3)}{\phi\mu^*/2\kappa^*(\overline{I}_{\mathrm{C}} - 3) + ((1-\phi)\mu^*)/2\kappa^*(\overline{II}_{\mathrm{C}} - 3) + 1/2(\sqrt{III_{\mathrm{C}}} - 1)^2} \right| \leqslant \left| \frac{\Delta\mu^*}{\mu^*} \right| \\ \operatorname*{Lim}_{III_{\mathrm{C}} \to 0} |\overline{\xi_{\mu^*}}| = \left| \frac{\Delta\mu^*}{\mu^*} \right|, \quad \operatorname*{Lim}_{III_{\mathrm{C}} \to \infty} |\overline{\xi_{\mu^*}}| = 0 \end{gathered}} \tag{16}$$

In other words, the normalized sensitivity of the energetic responses in the finite deformation range is never greater than the normalized sensitivity in the infinitesimal range. The energy sensitivities will attain the ratios $\Delta\mu^*/\mu$ and $\Delta\kappa^*/\kappa$, respectively, but at different extreme loading states.

4.2. Bounds on the perturbed Cauchy stresses

The corresponding second Piola–Kirchhoff stress tensor for the stored energy function employing effective constants in Equation (6) is

$$\begin{aligned} \mathbf{S} = 2 \Bigg(& K_1^* III_{\mathrm{C}}^{-1/3} \mathbf{I} + K_2^* III_{\mathrm{C}}^{-2/3} (I_{\mathrm{C}} \mathbf{I} - \mathbf{C}) \\ & + \left(\frac{\kappa^*}{2}(III_{\mathrm{C}} - III_{\mathrm{C}}^{1/2}) - \frac{K_1^*}{3} I_{\mathrm{C}} III_{\mathrm{C}}^{-1/3} - \frac{2K_2^*}{3} II_{\mathrm{C}}\, III_{\mathrm{C}}^{-2/3} \right) \mathbf{C}^{-1} \Bigg) \end{aligned} \tag{17}$$

The sensitivity of the Cauchy stresses can be obtained from the same transformation as between $\mathbf{S}$ and $\boldsymbol{\sigma}$, i.e. $\boldsymbol{\sigma} = (1/J)\mathbf{F} \cdot \mathbf{S} \cdot \mathbf{F}^{\mathrm{T}}$

$$\frac{\partial \boldsymbol{\sigma}}{\partial \kappa^*} = \frac{1}{J}\mathbf{F} \cdot \frac{\partial \mathbf{S}}{\partial \kappa^*} \cdot \mathbf{F}^{\mathrm{T}}, \quad \frac{\partial \boldsymbol{\sigma}}{\partial \mu^*} = \frac{1}{J}\mathbf{F} \cdot \frac{\partial \mathbf{S}}{\partial \mu^*} \cdot \mathbf{F}^{\mathrm{T}} \tag{18}$$

Therefore, we have

$$\boldsymbol{\sigma}(\kappa^* + \Delta\kappa^*) - \boldsymbol{\sigma}(\kappa^*) = \frac{\partial \boldsymbol{\sigma}}{\partial \kappa^*}\Delta\kappa^*, \quad \boldsymbol{\sigma}(\mu^* + \Delta\mu^*) - \boldsymbol{\sigma}(\mu^*) = \frac{\partial \boldsymbol{\sigma}}{\partial \mu^*}\Delta\mu^* \tag{19}$$

When these quantities are normalized, for example by the appropriate Cauchy stress components, they behave essentially in the same manner as the normalized energy sensitivities. In fact we have

$$\frac{\partial \mathbf{S}}{\partial \kappa^*} = (III_{\mathrm{C}} - III_{\mathrm{C}}^{1/2})\mathbf{C}^{-1} \tag{20}$$

and

$$\begin{aligned}\frac{\partial \mathbf{S}}{\partial \mu^*} = {} & \phi\left(III_{\mathrm{C}}^{-1/3}\mathbf{I} - \tfrac{1}{3}I_{\mathrm{C}}III_{\mathrm{C}}^{-1/3}\mathbf{C}^{-1}\right) \\ & + (1-\phi)\left(III_{\mathrm{C}}^{-2/3}(I_{\mathrm{C}}\mathbf{I} - \mathbf{C}) - \tfrac{2}{3}II_{\mathrm{C}}III_{\mathrm{C}}^{-2/3}\mathbf{C}^{-1}\right)\end{aligned} \tag{21}$$

After some straightforward algebra, we have ($\|\boldsymbol{\sigma}\| \stackrel{\text{def}}{=} (\boldsymbol{\sigma} : \boldsymbol{\sigma})^{1/2}$):

$$\boxed{\begin{aligned}\frac{\|(\partial\boldsymbol{\sigma}/\partial\kappa^*)\Delta\kappa^*\|}{\|\boldsymbol{\sigma}\|} &\leqslant \left|\frac{\Delta\kappa^*}{\kappa^*}\right| \\ \frac{\|(\partial\boldsymbol{\sigma}/\partial\mu^*)\Delta\mu^*\|}{\|\boldsymbol{\sigma}\|} &\leqslant \left|\frac{\Delta\mu^*}{\mu^*}\right|\end{aligned}} \tag{22}$$

where

$$\left\|\frac{\partial \boldsymbol{\sigma}}{\partial \kappa^*}\Delta\kappa^*\right\| \stackrel{\text{def}}{=} \left(\left(\frac{\partial \boldsymbol{\sigma}}{\partial \kappa^*}\Delta\kappa^*\right) : \left(\frac{\partial \boldsymbol{\sigma}}{\partial \kappa^*}\Delta\kappa^*\right)\right)^{1/2} \tag{23}$$

and

$$\left\|\frac{\partial \boldsymbol{\sigma}}{\partial \mu^*}\Delta\mu^*\right\| \stackrel{\text{def}}{=} \left(\left(\frac{\partial \boldsymbol{\sigma}}{\partial \mu^*}\Delta\mu^*\right) : \left(\frac{\partial \boldsymbol{\sigma}}{\partial \mu^*}\Delta\mu^*\right)\right)^{1/2} \tag{24}$$

4.3. Examples

We now provide some quantitative examples. Consider a block of material where we specify boundary displacements of the following form:

$$\mathbf{u}|_{\partial\Omega} = \mathscr{E} \cdot \mathbf{X} \Rightarrow \mathbf{F} = \mathbf{I} + \nabla_X \mathbf{u} = \mathbf{I} + \mathscr{E} \tag{25}$$

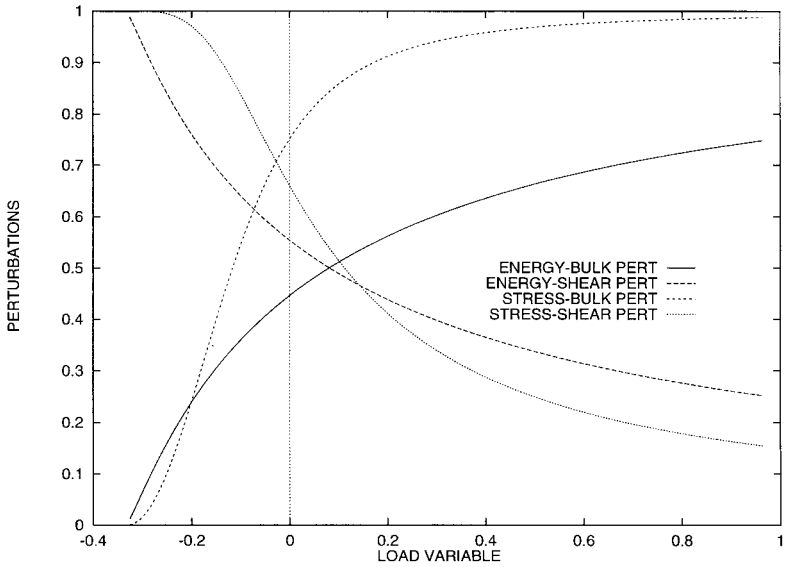

Figure 9. Multiaxial loading ($\phi = 0.5$): the behaviour of the perturbations $(\overline{\eta_{W-\kappa^*}}, \overline{\eta_{W-\mu^*}}, \overline{\eta_{\sigma-\kappa^*}}, \overline{\eta_{\sigma-\mu^*}})$ with multiaxial loading.

The following normalized quantities are important to illustrate the theoretical results:

$$\boxed{\begin{aligned} \overline{\eta_{W-\kappa^*}} &\stackrel{\text{def}}{=} \frac{\frac{\|(\partial W/\partial \kappa^*)\Delta\kappa^*\|}{W}}{|\Delta\kappa^*/\kappa^*|} \leqslant 1, \quad \overline{\eta_{W-\mu^*}} \stackrel{\text{def}}{=} \frac{\frac{\|(\partial W/\partial \mu^*)\Delta\mu^*\|}{W}}{|\Delta\mu^*/\mu^*|} \leqslant 1 \\ \overline{\eta_{\sigma-\kappa^*}} &\stackrel{\text{def}}{=} \frac{\frac{\|(\partial \boldsymbol{\sigma}/\partial \kappa^*)\Delta\kappa^*\|}{\|\boldsymbol{\sigma}\|}}{|\Delta\kappa^*/\kappa^*|} \leqslant 1, \quad \overline{\eta_{\sigma-\mu^*}} \stackrel{\text{def}}{=} \frac{\frac{\|(\partial \boldsymbol{\sigma}/\partial \mu^*)\Delta\mu^*\|}{\|\boldsymbol{\sigma}\|}}{|\Delta\mu^*/\mu^*|} \leqslant 1 \end{aligned}} \tag{26}$$

We now illustrate the behaviour of these quantities for three distinct loading cases: (1) multiaxial loading, (2) tensile loading and (3) shear loading.

4.3.1. Multiaxial loading. Consider the following multiaxial loading:

$$\begin{bmatrix} u_1|_{\partial\Omega} \\ u_2|_{\partial\Omega} \\ u_3|_{\partial\Omega} \end{bmatrix} = \alpha \begin{bmatrix} 1 & 1 & 1 \\ 1 & 1 & 1 \\ 1 & 1 & 1 \end{bmatrix} \begin{bmatrix} X_1 \\ X_2 \\ X_3 \end{bmatrix} \tag{27}$$

It is easy to show that $\alpha = -\frac{1}{3} \Rightarrow J = 0$, thus we restrict our view to $\alpha > -\frac{1}{3}$. The quantities of interest in Box (26) are shown in Figure 9, and are less than unity as theoretically predicted.

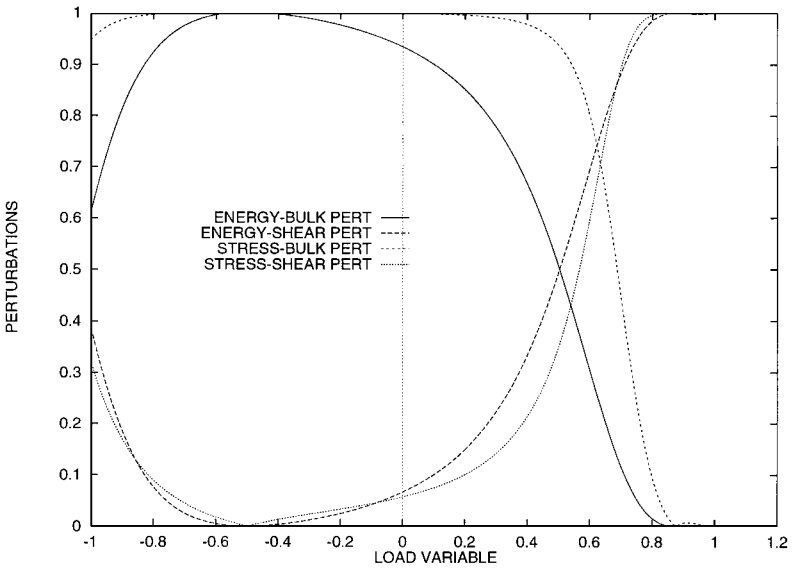

Figure 10. Tensile loading ($\phi = 0.5$): the behaviour of the perturbations $(\overline{\eta_{W-\kappa^*}}, \overline{\eta_{W-\mu^*}}, \overline{\eta_{\sigma-\kappa^*}}, \overline{\eta_{\sigma-\mu^*}})$ with multiaxial loading.

4.3.2. Tensile loading. Consider the following tensile loading:

$$\begin{bmatrix} u_1|_{\partial\Omega} \\ u_2|_{\partial\Omega} \\ u_3|_{\partial\Omega} \end{bmatrix} = \alpha \begin{bmatrix} 1 & 0 & 0 \\ 0 & 1 & 0 \\ 0 & 0 & 1 \end{bmatrix} \begin{bmatrix} X_1 \\ X_2 \\ X_3 \end{bmatrix} \tag{28}$$

For this case we have $\alpha = -1 \Rightarrow J = 0$, thus we restrict our view to $\alpha > -1$. The quantities of interest in Box (26) are shown in Figure 10.

4.3.3. Shear loading. Consider the following shear loading:

$$\begin{bmatrix} u_1|_{\partial\Omega} \\ u_2|_{\partial\Omega} \\ u_3|_{\partial\Omega} \end{bmatrix} = \alpha \begin{bmatrix} 0 & 1 & 1 \\ 1 & 0 & 1 \\ 1 & 1 & 0 \end{bmatrix} \begin{bmatrix} X_1 \\ X_2 \\ X_3 \end{bmatrix} \tag{29}$$

For this case, we have $\alpha = -\frac{1}{2}$ or $1 \Rightarrow J = 0$, thus we restrict our view to $1 > \alpha > -\frac{1}{2}$. The quantities of interest in Box (26) are shown in Figure 11.

Remark. As the theoretical results assert, in all three loading cases the perturbations in the finite deformation range are bounded by the perturbation ratio in the infinitesimal range.

5. CONCLUDING REMARKS

The widespread use of materials with heterogeneous microstructures in engineering applications has made their accurate characterization important. Deviations in macroscopic responses, perhaps

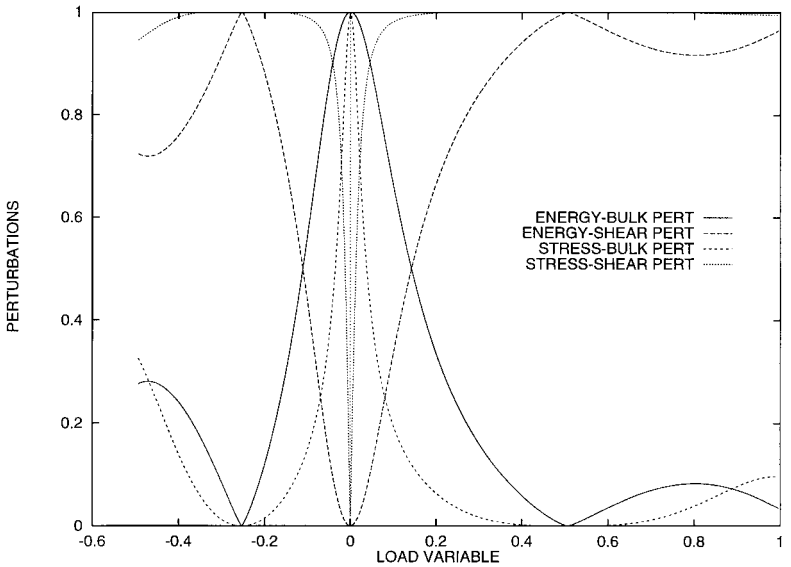

Figure 11. Shear loading ($\phi = 0.5$): the behaviour of the perturbations $(\overline{\eta_{W-\kappa^*}}, \overline{\eta_{W-\mu^*}}, \overline{\eta_{\sigma-\kappa^*}}, \overline{\eta_{\sigma-\mu^*}})$ with multiaxial loading.

produced from inaccurate material tests, can make large differences in the estimated performance and service life of structures. This is particularly relevant for porous polymers, which are widely used in modern engineering designs. In this work we were concerned with hyperelastic polyethelenes. For simplicity, we used a specific class of compressible Mooney–Rivlin response functions. It was shown that the perturbed response in the linear range bounds the resulting perturbed response in the finite deformation range from above. An analyses for more sophisticated models, for example Ogden response functions, is quite more involved. The authors are investigating whether the analysis presented here can be extended to obtain meaningful information for such functions, since they too are influenced by uncertainties in the linear elastic constants.

REFERENCES

1. Gibson L, Ashby M. *Cellular Solids. Structure and Properties* (2nd edn). Cambridge University Press: Cambridge, 1997.
2. Mura T. *Micromechanics of defects in Solids* (2nd edn). Kluwer Academic Publisher: Dordrecht, 1993.
3. Jikov VV, Kozlov SM, Olenik OA. *Homogenization of Differential Operators and Integral Functionals*. Springer: Berlin, 1994.
4. Zohdi TI, Feucht M, Gross D, Wriggers P. A description of macroscopic damage via microstructural relaxation. *International Journal for Numerical Methods in Engineering* 1998; **43**:493–507.
5. Huet C. Application of variational concepts to size effects in elastic heterogeneous bodies. *Journal of the Mechanics and Physics of Solids* 1990; **38**:813–841.
6. Huet C. Hierarchies and bounds for size effects in heterogeneous bodies. In *Continuum Models and Discrete Systems*, Maugin GA (ed.), vol. 2, Longman: Harlow, 1991; 127–134.
7. Hazanov S, Huet C. Order relationships for boundary conditions effect in heterogeneous bodies smaller than the representative volume. *Journal of the Mechanics and Physics of Solids* 1994; **42**:1995–2011.
8. Hazanov S, Amieur M. On overall properties of elastic heterogeneous bodies smaller than the representative volume. *International Journal of Engineering Science* 1995; **33**(9):1289–1301.
9. Zohdi TI, Wriggers P. A domain decomposition method for bodies with microstructure based upon material regularization. *International Journal of Solids and Structures* 1999; **36**(17):2507–2526.
10. Ciarlet PG. *Mathematical Elasticity*. Elsevier: Amsterdam, 1993.

